Physics

Physics Research Publications

Purdue University *Year* 2003

Improved tests of extra-dimensional physics and thermal quantum field theory from new Casimir force measurements

R. S. Decca E. Fischbach G. L. Klimchitskaya

D. E. Krause D. Lopez V. M. Mostepanenko

Improved tests of extra-dimensional physics and thermal quantum field theory from new Casimir force measurements

R. S. Decca,[1] E. Fischbach,[2,*] G. L. Klimchitskaya,[3,†] D. E. Krause,[4,2] D. López,[5] and V. M. Mostepanenko[3,‡]
[1]*Department of Physics, Indiana University–Purdue University Indianapolis, Indianapolis, Indiana 46202, USA*
[2]*Department of Physics, Purdue University, West Lafayette, Indiana 47907, USA*
[3]*Departamento de Física, Universidade Federal da Paraíba, Caixa Postal 5008, CEP 58059-970 João Pessoa, Paraíba, Brazil*
[4]*Physics Department, Wabash College, Crawfordsville, Indiana 47933, USA*
[5]*Bell Laboratories, Lucent Technologies, Murray Hill, New Jersey 07974, USA*
(Received 29 August 2003; published 11 December 2003)

We report new constraints on extra-dimensional models and other physics beyond the standard model based on measurements of the Casimir force between two dissimilar metals for separations in the range 0.2–1.2 μm. The Casimir force between a Au-coated sphere and a Cu-coated plate of a microelectromechanical torsional oscillator was measured statically with an absolute error of 0.3 pN. In addition, the Casimir pressure between two parallel plates was determined dynamically with an absolute error of $\approx$0.6 mPa. Within the limits of experimental and theoretical errors, the results are in agreement with a theory that takes into account the finite conductivity and roughness of the two metals. The level of agreement between experiment and theory was then used to set limits on the predictions of extra-dimensional physics and thermal quantum field theory. It is shown that two theoretical approaches to the thermal Casimir force which predict effects linear in temperature are ruled out by these experiments. Finally, constraints on Yukawa corrections to Newton's law of gravity are strengthened by more than an order of magnitude in the range 56–330 nm.

DOI: 10.1103/PhysRevD.68.116003 PACS number(s): 03.70.+k, 12.20.Ds, 12.20.Fv, 42.50.Lc

I. INTRODUCTION

Many extensions of the standard model, including supergravity and string theory, exploit the Kaluza-Klein idea that the true dimensionality of space-time is $N=4+n$, where the additional n spatial dimensions are compactified at some small length scale. For a long time it was generally believed that the compactification scale was on the order of the Planck length $l_{Pl}=\sqrt{G}\sim 10^{-33}$ cm, where G is the Newtonian gravitational constant, and units are chosen so that $\hbar=c=1$. The corresponding energy scale, $M_{Pl}=1/\sqrt{G}\sim 10^{19}$ GeV, is so high that direct experimental observation of the effects of extra dimensions would seem impossible at any time in the foreseeable future.

The situation changed dramatically with the proposal of models for which the compactification energy may be as low as the extra-dimensional Planck energy scale, $M_{Pl}^{(N)}=1/G_N^{1/(2+n)}$, which is assumed to be of the order of 1 TeV [1,2]. (Here G_N is the fundamental gravitational constant in the extended N-dimensional space-time.) Note that this proposal eliminates the hierarchy problem since the characteristic energy scales of gravitational and gauge interactions coincide. In order to be consistent with observations, the usual gauge fields of the standard model are presumed to exist on 4-dimensional branes whereas gravity alone propagates into the N-dimensional bulk.

Constraints on these new lower energy scale compactification models can be obtained by investigating their predictions in accelerator experiments [3–5], astrophysics [6–8], and cosmology [9–11]. More model-independent limits, however, can be obtained from tests of Newtonian gravity. In extra-dimensional models with large compact extra dimensions [1], the Newtonian gravitational potential acting between two point masses acquires a Yukawa correction for separations much larger than the compactification scale [12,13], while for models with non-compact but warped extra dimensions, the corrections are power laws [2]. For two interacting macroscopic bodies, either of these corrections would give rise to a new (so called ''fifth'') force coexisting with the usual Newtonian gravitational force and other conventional standard model interactions, such as Casimir and van der Waals forces. In addition, many extensions of the standard model that do not involve extra dimensions also predict the existence of new Yukawa or power-law forces.

While gravity experiments at ranges $\gtrsim 10^{-3}$ m have found no convincing evidence of new forces or extra dimensions, tests of Newtonian gravity over shorter separations were lacking until recently. During the past few years a number of sub-millimeter gravity experiments were performed and stronger constraints on Yukawa corrections to Newtonian gravity for ranges $\sim 10^{-4}$ m have been obtained [14–17]. For significantly smaller separations, however, gravity loses its role as the dominant force acting between non-magnetic, electrically neutral interacting bodies. For these smaller separations, limits on new forces and extra-dimensions from force measurements must be extracted from the Casimir and van der Waals forces [18] which increase rapidly as the separation decreases.

Improvements in the precision of Casimir force measurements coincided with the development of modern extra-

*Corresponding author.
†On leave from North-West Technical University, St. Petersburg, Russia.
‡On leave from Noncommercial Partnership ''Scientific Instruments,'' Moscow, Russia.

dimensional theories. To date a number of Casimir force experiments have been performed using different techniques [19–27], and a precision of 1.8% (at the 95% confidence level) of the measured force at the shortest separation distances has been achieved (see Ref. [28]). We note that the 1% precision quoted, e.g., in Refs. [20,21,23] corresponds to a 60% confidence level. To obtain good agreement between theory and experiment, it has been necessary to take into account corrections to the Casimir force due to finite conductivity of the boundary metals, surface roughness, and nonzero temperature [20,29–35].

Although these new precision measurements of the Casimir force were not especially designed or optimized to obtain stronger constraints on the predictions of extra-dimensional physics, some of them were used for this purpose [35–39]. This resulted in a strengthening of previously known constraints by a factor as large as 4500 in some regions within the range 10^{-9} m–10^{-4} m. This means that Casimir force measurements have become a powerful competitor to both accelerator and gravitational experiments in constraining theoretical models of high energy physics. In contrast to astrophysical and cosmological constraints, the results of Casimir force measurements are less model dependent, reproducible, and therefore more reliable.

In this paper we present detailed results of new, increased precision, Casimir force measurements between a Cu-coated plate and a Au-coated sphere (see Ref. [40] for preliminary data). The use of a microelectromechanical torsional oscillator (MTO) and of interferometric measurements of the sphere-plate separations permitted much higher sensitivity to be achieved than in previous Casimir force experiments. A careful error analysis has been performed, and the experimental precision was determined at the 95% confidence level. The complete theory of the Casimir force, taking into account finite conductivity and surface roughness corrections, has been applied to the experimental configuration. The finite conductivity corrections were computed by the use of the Lifshitz formula [41] and tabulated optical data for the complex index of refraction. The surface roughness was modelled using atomic force microscope (AFM) images of the interacting surfaces. A comparison of the complete theory with experimental data shows that they are in agreement over the whole measurement range. A minor disagreement at the shortest separations noted in Ref. [40] is explained by the incomplete theory of roughness corrections used in the earlier analysis.

Our results were sufficiently precise to shed light on the temperature dependence of the Casimir force. Several theories predicting large thermal corrections to the Casimir force at small separations [42–44] were evaluated for our experiment. It is well known that these corrections disagree with the results obtained for ideal metals in the framework of quantum field theory at nonzero temperature in the Matsubara formulation. Our experimental data support the results of Refs. [32,33], which are consistent with the conclusions of thermal quantum field theory, while ruling out the existence of large thermal corrections at small separations as proposed in Refs. [42,43] and in Ref. [44].

Finally, the experimental results presented here are used to constrain the predictions of extra-dimensional physics in the nanometer separation range. The contributions from a Yukawa-type hypothetical force have been calculated for our experimental configuration, taking into account the effects of surface roughness. The agreement between theoretical and measured values of the Casimir force leads to the strengthening of the known constraints on Yukawa forces by a factor of up to 11 within the 56–330 nm interaction range. In contrast to some previous constraints derived from Casimir force measurements, it is possible here to quantify the confidence level of the obtained results.

This paper is organized as follows. In Sec. II the experimental configurations used for both static and dynamic measurements of the Casimir force are described. Section III presents the experimental results with a discussion of their precision. In Sec. IV we calculate the Casimir force taking into account all relevant corrections. Section V is devoted to the determination of the theoretical precision, the comparison of experimental results with theory, and to the evaluation of alternative methods for taking into account thermal corrections. In Sec. VI we use our results to obtain constraints on hypothetical forces predicted by models of extra-dimensional physics and extensions of the standard model. We conclude with Sec. VII which summarizes all of our results.

II. EXPERIMENTAL ARRANGEMENT FOR STATIC AND DYNAMIC MEASUREMENTS

In our experiment, the Casimir force between two dissimilar metals (gold and copper) was measured using a MTO operating in both static and dynamic modes. In the static regime the Casimir force between a Au-coated sphere and a Cu-coated plate of the MTO was measured. In the dynamic regime the vertical separation between the sphere and the plate was changed harmonically with time. This leads to a measurement of the z derivative of the Casimir force, which is equivalent to measuring the Casimir force per unit area, or the Casimir pressure, for a configuration of two parallel plates (see below). Note that the dynamic measurement technique is used here to measure the usual (static) Casimir effect. Hence, this measurement is unrelated to the so-called dynamic Casimir effect which arises from the velocity dependent Casimir forces or the creation of photons by the rapidly oscillating plates [35].

When using mechanical oscillators to measure forces, one has to confront the coupling of the oscillator with environmental vibrations. Compared with cantilever oscillators, torsional oscillators are less sensitive to mechanical vibrations that induce a motion of the center of mass. Furthermore, the miniaturization of the oscillators yields an improvement in its quality factor and sensitivity [25,45]. It is consequently advantageous to use an electromechanical torsional oscillator to measure the Casimir force between two metals.

The experimental arrangement is shown schematically in Fig. 1. The MTO is made of a 3.5 μm thick, 500 $\times$500 μm^2 heavily doped polysilicon plate suspended at two opposite points by serpentine springs, as shown in the inset of Fig. 2. The springs are anchored to a silicon nitride (SiN_x)

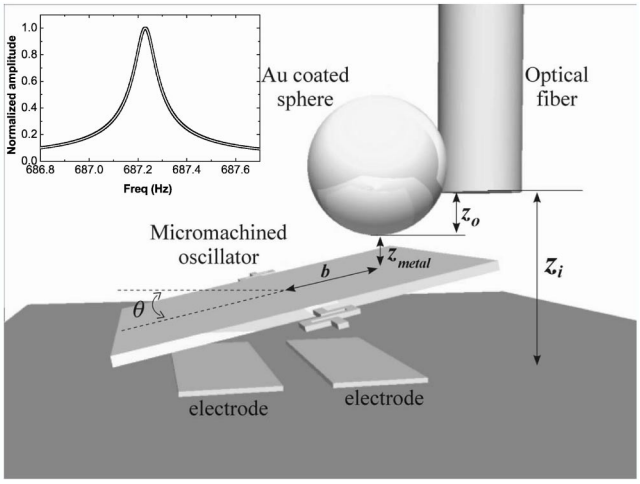

FIG. 1. Schematic of the experimental setup showing its main components, see text. Inset: Resonance curve for the MTO. Also shown is a Lorentzian fit with $Q\sim 8000$. See text for further details.

covered Si platform. When no torques are applied the plate is separated from the platform by a gap ~ 2 μm. Two independently contacted polysilicon electrodes located under the plate are used to measure the capacitance between the electrodes and the plate. For the MTO employed in this experiment, we calculated the torsion coefficient $\kappa = (wt^3 E_{Si}/6L_{serp}) \simeq 9.5\times 10^{-10}$ Nm/rad [46], where $w = 2$ μm is the width of the serpentine, $t = 2$ μm is its thickness, $L_{serp} = 500$ μm its length, and $E_{Si} = 180$ GPa is Young's modulus for Si. This value is in good agreement with the measured value $\kappa = 8.6\times 10^{-10}$ N m/rad. The edges of the plate are coated with 1 nm of Cr followed by 200 nm of Cu. This layer of Cu constitutes one of the metals used in the measurement of the Casimir force.

The remainder of the assembly, as shown in Fig. 1, consists of a Au-coated Al_2O_3 sphere that can be brought in close proximity to the Cu-coated plate. Al_2O_3 spheres with nominal diameters ranging from 100 μm to 600 μm were coated with a ~ 1 nm layer of Cr followed by a ≈ 203 nm

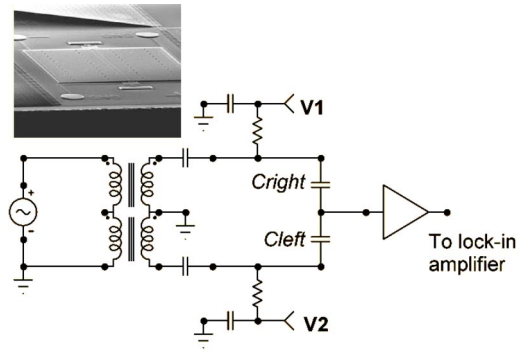

FIG. 2. Schematic of the bridge circuit used to measure the capacitance. The dc voltages V_1 and V_2 are used to correct for small deviations when no interactions are present. They also linearize the response of the circuit. Details of the charge amplifier and the part of the circuit used to balance the bridge are omitted for clarity. Inset: Scanning electron microscopy image of the MTO.

layer of gold. The coated sphere used in the experiment was subsequently glued with conductive epoxy to the side of a Au-coated optical fiber, establishing an electrical connection between them. The sphericity of the Al_2O_3 balls, as measured on a scanning electron microscope (SEM), was found to be within the specifications of the manufacturer. As an example, a 600-μm-diameter ball was found to have an ellipsoidal shape with major and minor semi-axes of (298 ± 2) μm and (294.0 ± 0.5) μm, respectively. For the sake of clarity we will refer to the ball as a sphere in the remainder of the paper. Deposition induced asymmetries were found to be smaller than 10 nm, the resolution of the SEM. The entire setup (MTO and fiber sphere) was rigidly mounted into a can, where a pressure $\lesssim 10^{-4}$ torr was maintained. The can has built-in magnetic damping vibration isolation and was, in turn, mounted onto an air table. This combination of vibration isolation systems yielded base vibrations with $\Delta z^{rms} < 0.05$ nm for frequencies above 100 Hz.

The fiber-sphere assembly was moved vertically by the combination of a micrometer-driven and a piezo-driven stage. The MTO was mounted on a piezoelectric driven xyz stage which, in turn, is mounted on a micrometer controlled xy stage. This combination allows positioning the Au-coated sphere over the Cu-coated plate. The separation z_i between the sphere and the Si platform was controlled by the z axis of the xyz stage. A two color fiber interferometer-based closed-loop system was used to keep z_i constant. The error in the interferometric measurements was found to be $\Delta z_i^{rms} = 0.32$ nm, dominated by the overall stability of the closed-loop feedback system. Since this error is much greater than the actual mechanical vibrations of the system, the closed loop was turned off while data acquisition was in progress.

The separation z_{metal} between the two metallic surfaces (see Fig. 1) is given by $z_{metal} = z_i - z_0 - z_g - b\theta$, where b is the lever arm between the sphere and the axis of the MTO, and θ is the angle between the platform and the plate ($\theta \ll 1$ has been used). z_0 is the distance the bottom of the sphere protrudes from the end of the cleaved fiber, and z_g includes the gap between the platform and the plate, the thickness of the plate, and the thickness of the Cu layer. An initial characterization of z_0, by alternately gently touching the platform with the sphere and the bare fiber yielded $z_0 = (55.07\pm 0.07)$ μm. Also, $z_g = (5.73\pm 0.08)$ μm was determined using an AFM. Since errors in z_g and z_0 propagate to z_{metal}, it is necessary to provide a better characterization, which is described below.

A force $F(z)$ acting between the sphere and the plate produces a torque $\tau = bF(z) = \kappa\theta$ on the plate. (In all cases reported in this paper $\theta \leqslant 10^{-5}$ rad, so $\theta \ll 1$.) Under these circumstances $\theta \propto \Delta C = C_{right} - C_{left}$, where C_{right} (C_{left}) is the capacitance between the right (left) electrode and the plate (Fig. 1). Consequently the force between the two metallic surfaces separated by a distance z is $F(z) = k\Delta C$, where k is the proportionality constant. The capacitance was measured using the circuit schematically shown in Fig. 2 [47]. The 10 nV/Hz$^{1/2}$ electronic noise of the amplifier stage is equivalent to an angular deviation $\delta\theta \sim 10^{-9}$ rad/Hz$^{1/2}$.

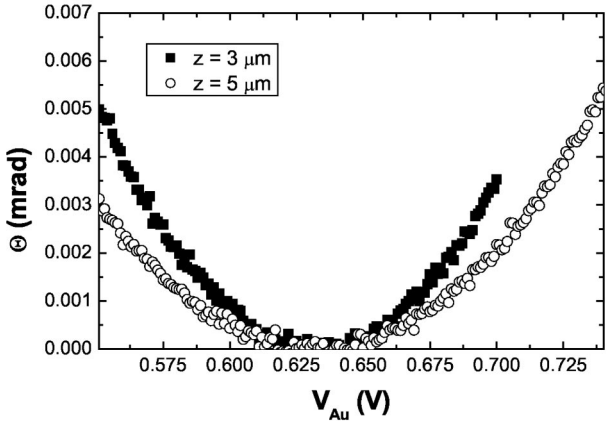

FIG. 3. Dependence of the angular deviation θ as a function of the applied voltage to the sphere. Data obtained at two different separations z between the metallic layers are shown.

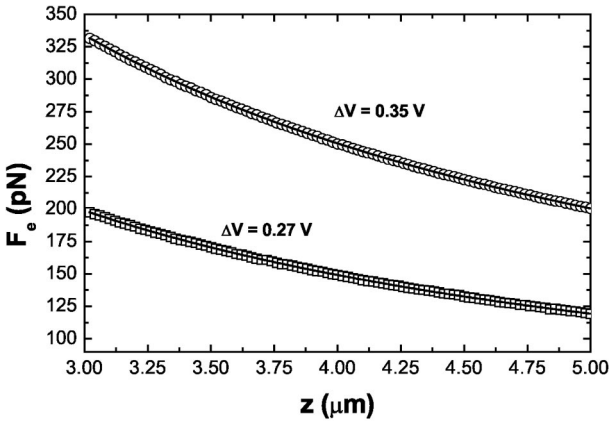

FIG. 4. Electrostatic force F_e as a function of separation z for $\Delta V = V_{\rm Au} - V_0 = 0.27$ V and $\Delta V = 0.35$ V. The fits of the data using Eq. (2) are also shown by the solid lines. See text for further discussion.

This noise level is much smaller than the thermodynamic noise at the measuring frequency $f = 10$ kHz $\gg f_0 = 687.23$ Hz [48],

$$S_\theta^{1/2} = \left[\frac{2k_B TQ}{\pi f_0 \kappa}\left(\frac{f_0}{f}\right)^2\right]^{1/2} \simeq 3\times 10^{-7}\,\text{rad/Hz}^{1/2}, \qquad (1)$$

where k_B is Boltzmann's constant, $T = 300$ K, and the quality factor $Q \simeq 8000$. (See the inset of Fig. 1.) Using these values a force sensitivity $\delta F = \kappa S_\theta^{1/2}/b \simeq 1.4$ pN/Hz$^{1/2}$ is obtained.

To provide a calibration of the proportionality constant k between F and ΔC, we applied a known potential difference between the Au-coated sphere and the Cu film. This was done at $z_{metal} > 3$ μm, in configurations where the contribution from the Casimir force is smaller than 0.1% of the total force. Thus, the net force can be approximated by retaining only the electrostatic force F_e between a sphere and an infinite plane [49],

$$F_e = 2\pi\epsilon_0 (V_{\rm Au} - V_0)^2 \sum_{n=1}^{\infty} \frac{[\coth(u) - n\coth(nu)]}{\sinh(nu)}. \qquad (2)$$

Here ϵ_0 is the permittivity of free space, $V_{\rm Au}$ is the voltage applied to the sphere, V_0 is the residual potential difference between the metallic layers when they are both grounded, and $\cosh u = [1 + z/R]$, with $z = z_{metal} + 2\delta_0$ (R is the radius of the sphere). $2\delta_0$ is the average separation between the metal layers when the test bodies come in contact (so that $z_{metal} = 0$), and is primarily determined by the roughness of the films. Although the profile of the roughness does not affect the value of the electric force at large separations, its presence should be taken into account in the determination of the separation between the smoothed out surfaces. In Eq. (2) it was found that only the first two terms of the z/R expansion gave a significant contribution. Figure 3 shows the dependence of θ (and hence the electrostatic force) on the applied voltage $V_{\rm Au}$. The minimum in the force was found to occur when $V_0 = (632.5 \pm 0.3)$ mV, which reflects the difference in the work functions of the Au and Cu layers. This value was observed to be constant for z in the 0.2–5 μm range and it did not vary when measured over different locations in the Cu layer.

Once the value V_0 was found, Eq. (2) was used to determine three different parameters: (i) the proportionality constant k between the sphere-plate force and the measured difference in capacitances; (ii) the radius R of the coated sphere; and (iii) the increase in the separation $2\delta_0$ between the two metallic layers. Two of the curves obtained in the 3–5 μm range are shown in Fig. 4. A simultaneous fit to more than 100 such curves yields $k = (50280 \pm 6)$ N/F, $R = (294.3 \pm 0.1)$ μm, and $\delta_0 = (39.4 \pm 0.3)$ nm.

The above force sensitivity can be improved by performing a dynamic measurement which directly uses the high quality factor of the MTO [25]. In this approach, the separation between the sphere and the oscillator was varied as $\Delta z_{metal} = A\cos(\omega_r t)$, where ω_r is the resonant angular frequency of the MTO, and A was adjusted between 3 and 35 nm for values of z_{metal} between 0.2 and 1.2 μm, respectively. The solution for the oscillatory motion yields [25],

$$\omega_r^2 = \omega_0^2\left[1 - \frac{b^2}{I\omega_0^2}\frac{\partial F_C}{\partial z}\right], \qquad (3)$$

where $\omega_0 \simeq \sqrt{\kappa/I}$ for $Q \gg 1$, $I \simeq 4.6\times 10^{-17}$ kg m^2 is the moment of inertia of the oscillator, and F_C is the Casimir force between the sphere and the plate. Since $A \ll z_{metal}$, terms of higher order in $\partial F_C/\partial z$ introduce a $\sim 0.1\%$ error at separations $z \geqslant 250$ nm. As before, Eq. (2) was used to calibrate all constants. We found $\omega_0 = 2\pi \times 687.23$ Hz, and $b^2/I = 1.2978\times 10^9$ kg^{-1}. With an integration time of 10 s using a phase-lock-loop circuit [50], changes in the resonant frequency of 10 mHz were detectable.

The main source of error for the frequency measurement, $\delta f = 10$ mHz, is the error in the trigger of the frequency meter. This error δt originated in the jitter of the signal due to the relatively large thermodynamic noise-induced $\delta\theta$ observed at resonance [48]. This dominant noise is

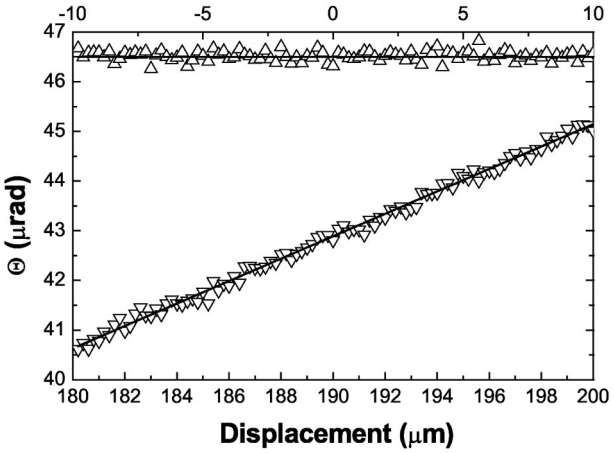

FIG. 5. Angular displacement of the MTO as a function of linear displacement when the sphere is moved parallel to the MTO's axis (top axis, $\triangle$) and when it is moved perpendicular to the MTO's axis (bottom axis, $\triangledown$). The data were acquired at $z=3$ μm with $\Delta V=0.27$ V. For comparison, the expected values for an infinite Cu layer using Eq. (2) are shown as solid lines.

$$\delta f = \frac{\sqrt{16} f^{3/2} \delta t}{\sqrt{\Upsilon}}, \tag{4}$$

where Υ is the integration time.

Unlike the static regime where forces are measured, in the dynamic regime the force gradient $\partial F_C/\partial z$ is measured using Eq. (3) by observing the change in the resonant frequency as the sphere-plate separation changes. According to the proximity force theorem [51,52],

$$F_C(z) = 2\pi R E_C(z), \tag{5}$$

where $E_C(z)$ is the Casimir energy per unit area for two infinitely large parallel plates composed of the same materials as the sphere and plate (see Sec. IV for details). Differentiating Eq. (5) with respect to z one obtains

$$-\frac{\partial F_C(z)}{\partial z} = 2\pi R P_C(z), \tag{6}$$

where $P_C(z)$ is the force per unit area between two infinite plates. Thus, in the dynamic regime the Casimir force gradient between the sphere and plate can be directly related to the Casimir pressure between two infinite parallel plates composed of the same materials. Since the formula for the Casimir pressure for the parallel plate configuration is readily obtained, it proves more convenient to use Eq. (6) to express the results for the dynamic measurements in terms of the parallel plate pressure P_C instead of the force derivative $\partial F_C/\partial z$. From Eq. (4), the error in the measurement of the frequency translates into an equivalent pressure sensitivity given by $\delta P_C \simeq 4\times 10^{-4}$ Pa/Hz$^{1/2}$.

Finally, one additional test was performed, in this case to analyze the influence of the finite extent of the Cu layer on the measured forces. The analysis was done using, once again, the electrostatic force given by Eq. (2). Figure 5 shows the relevant data. When the sphere was moved parallel to the axis of the oscillator over 20 μm no change in θ was observed. When the motion was instead perpendicular to the axis of the oscillator the dependence expected from Eq. (2) was obtained within the experimental error. We thus conclude that there are no significant deviations from the assumption that the Cu plane is of infinite extent.

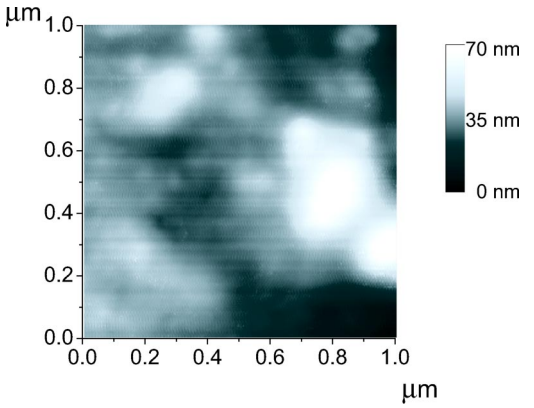

FIG. 6. 1×1 μm^2 atomic force microscopy image of the Cu layer. The topography of the Au layer on the sphere is similar. The gray scale to the right of the image gives the height of peaks above the bottom of roughness, with lighter tones corresponding to larger heights. The set of such images was used to analyze the effect of the surface roughness on the Casimir force as described in the text.

III. EXPERIMENTAL RESULTS AND THEIR PRECISION

A. Surface roughness of samples

The electric force measurements used to calibrate the apparatus were performed at large separations so that the Casimir force could be neglected, and the plate-sphere separation was calibrated between the middle levels of the surface roughness. By contrast, the Casimir force at small separations depends sensitively on the profile of the surface roughness, and hence the surface roughness should be carefully analyzed and characterized. The topography of the metallic films was investigated using an AFM probe with a radius of curvature $r_c=5$ nm in tapping mode. Regions of the metal plate and the sphere varying in size from 1 μm$\times$1 μm to 10 μm$\times$10 μm were scanned. A typical surface scan of a 1 μm$\times$1 μm region is shown in Fig. 6, where the lighter tone corresponds to higher regions. As seen in Fig. 6, the major distortions are the large mounds situated irregularly on the surface. Also noticeable in Fig. 6 are streaks which arise from high frequency noise with amplitude $h^{rms}\sim 1$ nm. This noise is caused by the oscillation of the free-standing MTO while acquiring AFM images.

In order to include the effects of surface roughness in the Casimir force calculations, the fraction of the surface area v_i with height h_i is needed. Data resulting from the most representative scan of a 10 μm$\times$10 μm region are shown in Fig. 7. The heights h_i are plotted along the vertical axis as a function of the fraction w_i of the total surface area having height less than h_{i+1}. The width of each horizontal step is equal to the fraction of the total area v_i with heights $h_i \leqslant h < h_{i+1}$. For example, regions with heights $h < h_2 = 8.2$ nm

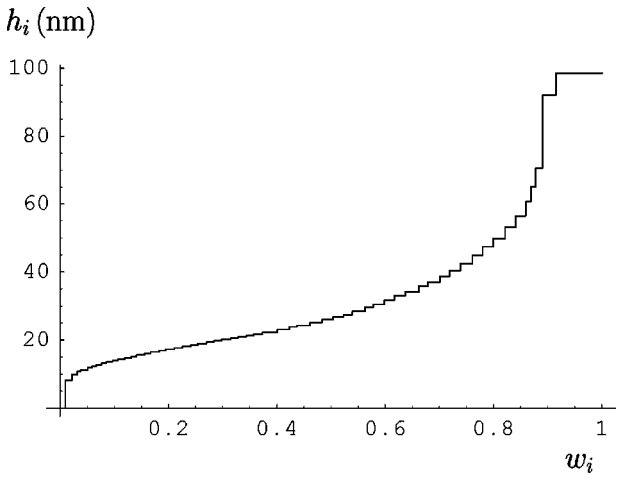

FIG. 7. Relief heights h_i vs the fraction of the total area with heights $h<h_{i+1}$.

are referred to the first (bottom) distortion level $h_1=0$ with $v_1=0.0095$, and regions with heights $h_2\leqslant h<h_3=9.87$ nm are referred to the second distortion level h_2 with $v_2=0.0121$. Regions with heights $h\geqslant h_{59}=98.5$ nm are referred to h_{59}, and occupy a fraction $v_{59}=0.085$ of the total area. Evidently $w_i=v_1+v_2+\cdots+v_i$, and $w_{59}=1$.

The data of Fig. 7 will be used in Sec. IV for the computation of the Casimir force taking into account roughness corrections (in Ref. [40] a simplified model of roughness was used). These data are also required for the precise determination of the so-called zero roughness level H_0 relative to which the mean value of the function, describing the total roughness, is zero. For convenience, in comparison with theory, all separation distances in the Casimir force measurements presented below are measured between the zero roughness levels.

The zero roughness level H_0 is found using the equality

$$\sum_{i=1}^{59}(h_i-H_0)v_i=0. \tag{7}$$

By combining the data of Fig. 7 with Eq. (7), one finds $H_0\approx 35.46$ nm. It is seen that the zero roughness level is slightly different from the quantity $\delta_0\approx 39.4$ nm, the correction to the separation on contact determined by the results of the electric force measurements (see Sec. II). The separation distances between zero roughness levels $z=d-2H_0$ used below (d is the separation between the bottom roughness levels) are larger by $2(\delta_0-H_0)=7.88$ nm than the separations $d-2\delta_0$ defined by the electric force measurements. (The difference between H_0 and δ_0 can be explained by a minor modification of the highest roughness peaks before the beginning of the Casimir force measurements.)

B. Static measurements of the Casimir force

To measure the Casimir force in the static regime, the bridge (schematically shown in Fig. 2) was first balanced using two identical capacitors replacing the MTO. Then the MTO was put back in place and the voltages V_1 and V_2 adjusted to give a null signal. This last adjustment is required to take into account residual asymmetries in the MTO. It was found that the difference between V_1 and V_2 corresponded to a variation in z, $\delta z\leqslant 6$ nm. Once the MTO was mounted and the can was evacuated, the sphere was brought into proximity with the MTO and the electrostatic measurements were performed. Without breaking the vacuum in the system the Casimir force measurements were then carried out. Figure 8 shows one such data set out of 19 runs. Each data point was obtained with an integration time of 10 s, a time interval which represents a good compromise for the ≈ 300 data points taken per run. It is worth mentioning, however, that the force sensitivity can be improved by using longer integration times.

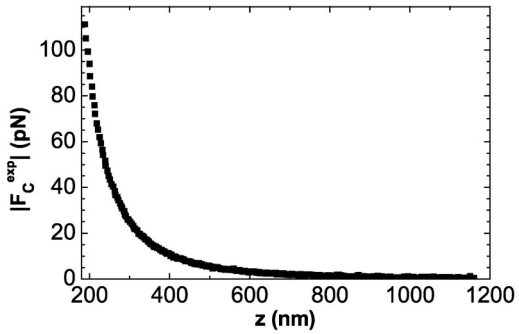

FIG. 8. Absolute value of the measured Casimir force as a function of separation obtained using the static mode. The value of the separation between the two metals is determined as discussed in the text.

The following analysis of the experimental precision is based on all $n=19$ series of measurements. For this purpose we calculate the mean values of the measured Casimir force

$$\overline{F}_C^{exp}(z_m)=\frac{1}{n}\sum_{i=1}^{n}F_{C,i}^{exp}(z_m) \tag{8}$$

at different separations z_m within the measurement separation range from 190 nm to ≈ 1.15 μm. The mean square error of $\overline{F}_C^{exp}$ is equal to

$$s_n(z_m)=\left\{\frac{1}{n(n-1)}\sum_{i=1}^{n}[\overline{F}_C^{exp}(z_m)-F_{C,i}^{exp}(z_m)]^2\right\}^{1/2}. \tag{9}$$

Our calculations show that $s_n(z_m)$ does not depend sensitively on m. The largest value $s_n=0.143$ pN can be taken as the value of the mean square error of $\overline{F}_C^{exp}$ within the whole measurement range. Taking into account that at $\alpha=95\%$ confidence level the Student's coefficient is $t_{\alpha,n}=2.1$, one obtains for the random absolute error of the Casimir force measurements in the static regime

$$\Delta_{st}^{rand}F_C^{exp}=s_n t_{\alpha,n}\approx 0.3 \text{ pN}. \tag{10}$$

In fact this effectively gives the total absolute error $\Delta_{st}^{tot}F_C^{exp}$ since the systematic errors are far below 0.1 pN for an integration time of 10 s. As a result, at the shortest separation of

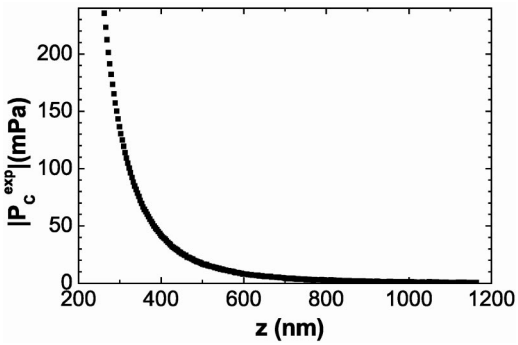

FIG. 9. Absolute value of the parallel plate Casimir pressure as a function of separation obtained from the dynamic measurement. The value of the separation between the two metals is determined as discussed in the text.

about 188 nm the relative error of the Casimir force measurement is 0.27%. We note that the true value of the Casimir force at a separation z lies in the confidence interval

$$[\overline{F}_C^{exp}(z)-\Delta_{st}^{tot}F_C^{exp},\overline{F}_C^{exp}(z)+\Delta_{st}^{tot}F_C^{exp}]$$

with a probability of 95%.

C. Dynamic measurements of the Casimir pressure

The results for the parallel plate Casimir pressure in the dynamic regime are shown in Fig. 9, which presents one dataset of 5 runs. Although the measurement was extended down to a separation of $\sim$180 nm, only data for separations above 260 nm are plotted. Data points below 260 nm show effects of nonlinear behavior of the oscillator [25].

The error analysis is performed in the same way as for the static regime. For $l=5$ runs, with $\approx$300 points per run, the largest mean square error is found to be $s_l=0.11$ mPa. The Student's coefficient at $\alpha=95\%$ confidence level is $t_{\alpha,l}=2.8$ leading to a random absolute error $\Delta_{dyn}^{rand}P_C^{exp}=0.31$ mPa. In the case of dynamic measurements, however, it is not possible to neglect systematic errors compared to random errors. As noted in Sec. II, there is an error $\delta\omega\approx 2\pi\times 10^{-2}$ Hz which from Eq. (3) leads to the absolute error in $\partial F_C/\partial z\approx 4.2\times 10^{-7}$ N/m. The latter, when combined with the error associated with the sphere's radius (equal to 0.1 μm), leads via Eq. (6) to a systematic error on the pressure $\Delta_{dyn}^{syst}P_C^{exp}$, which varies from 0.31 mPa at the shortest separation $z=260$ nm to 0.23 mPa at all separations $z\geqslant 450$ nm. As a result, the total absolute error of pressure measurements in the dynamic regime is equal to

$$\Delta_{dyn}^{tot}P_C^{exp}=\Delta_{dyn}^{rand}P_C^{exp}+\Delta_{dyn}^{syst}P_C^{exp}. \tag{11}$$

This error is z-dependent and varies from 0.62 mPa at $z=260$ nm to 0.54 mPa at $z\geqslant 450$ nm. Hence, the relative error of the Casimir pressure measurement at the shortest separation of about 260 nm is 0.26%.

IV. THEORETICAL DETERMINATION OF THE CASIMIR FORCE

A. Casimir force and pressure including finite conductivity

As described in Sec. II, the static and dynamic measurements were carried out using a Au-coated sphere over a Cu-coated plate. The thicknesses of both metal coatings were much larger than the plasma wavelength λ_p of both metals so that we can calculate the Casimir force as if the sphere and plate were composed of solid Au and Cu, respectively. As a first approximation, we consider the plate to have an infinite area. (Corrections due to the finite size of the plate will be estimated below.) The Casimir force between an infinite plate and a sphere (which was measured in the static regime, see Sec. II) can then be found using the Lifshitz formula for two plane parallel plates and the proximity force theorem [41,53],

$$F_C(z)=\frac{R}{2\pi}\int_0^\infty k_\perp dk_\perp\int_0^\infty d\xi\{\ln[1-r_\parallel^{(1)}(\xi,k_\perp)r_\parallel^{(2)}(\xi,k_\perp)\times e^{-2qz}]+\ln[1-r_\perp^{(1)}(\xi,k_\perp)r_\perp^{(2)}(\xi,k_\perp)e^{-2qz}]\}. \tag{12}$$

Here $q^2=k_\perp^2+\xi^2$, $k_\perp$ is the modulus of the wave vector in the plane of the plates, and $r_{\parallel,\perp}^{(l)}$ ($l=1,2$ for Cu, Au, respectively) are the reflection coefficients for two independent polarization states computed along the imaginary frequency axis $\omega=i\xi$. We note that the errors introduced by the proximity force theorem used to derive Eq. (12) are smaller than z/R [54,55]. This is a correction of less than 0.06% at the shortest separation distance, where the force measurements are most precise. (Recall that the experimental precision at $z=188$ nm was found to be 0.27%.) Equation (12) takes into account the finite conductivity corrections to the Casimir force due to real metal boundaries, but does not consider the effect of surface roughness and thermal corrections which will be treated later.

The reflection coefficients used in Eq. (12) can be represented in terms of either the dielectric permittivity or the surface impedance. In terms of the dielectric permittivity, as in the original Lifshitz formula (denoted by the subscript L), the reflection coefficients are given by

$$r_{\parallel,L}^{(l)}(\xi,k_\perp)=\frac{k^{(l)}-\varepsilon^{(l)}(i\xi)q}{k^{(l)}+\varepsilon^{(l)}(i\xi)q},\quad r_{\perp,L}^{(l)}(\xi,k_\perp)=\frac{q-k^{(l)}}{q+k^{(l)}}, \tag{13}$$

where $k^{(l)2}=k_\perp^2+\varepsilon^{(l)}(i\xi)\xi^2$. In terms of the surface impedance, the reflection coefficients are given by [34]

$$r_\parallel^{(l)}(\xi,k_\perp)=\frac{Z^{(l)}(i\xi)\xi-q}{Z^{(l)}(i\xi)\xi+q},\quad r_\perp^{(l)}(\xi,k_\perp)=\frac{Z^{(l)}(i\xi)q-\xi}{Z^{(l)}(i\xi)q+\xi}, \tag{14}$$

where $Z^{(l)}(i\xi)$ is the impedance for Cu or Au computed along the imaginary frequency axis.

It has been shown recently [34] that for real metals at nonzero temperature and interacting at relatively large separations, the representation described in Eq. (14) is preferable. It is free of contradictions with thermodynamics, which arise when reflection coefficients expressed by Eq. (13) are used in combination with the Drude dielectric function containing a nonzero relaxation parameter [56]. Within the experimental separation ranges of Sec. II (0.2–1.2 μm) the characteristic angular frequency of the Casimir effect $\omega_c = 1/(2z)$ lies within the region of infrared optics (using $c=1$), where the dielectric permittivity of the plasma model and the surface impedance along the imaginary frequency axis are given by

$$\varepsilon(i\xi) = 1 + \frac{\omega_p^2}{\xi^2}, \quad Z(i\xi) = \frac{\xi}{\sqrt{\omega_p^2 + \xi^2}}. \tag{15}$$

As demonstrated in [57] both formulations of the reflection coefficients, Eqs. (13) and (14), lead to the same computational results for the Casimir force, Eq. (12), when Eq. (15) is taken into account.

In the dynamic regime of Sec. II, the Casimir force gradient between the sphere and plate was measured. As shown above, this force gradient can be reexpressed in terms of the Casimir pressure acting between two parallel plates composed of the same materials. This Casimir pressure between parallel plates can also be represented in terms of the reflection coefficients

$$P_C(z) = -\frac{1}{2\pi^2}\int_0^\infty k_\perp dk_\perp \times \int_0^\infty q d\xi \left\{ \left[\frac{e^{2qz}}{r_\parallel^{(1)}(\xi,k_\perp) r_\parallel^{(2)}(\xi,k_\perp)} - 1 \right]^{-1} + \left[\frac{e^{2qz}}{r_\perp^{(1)}(\xi,k_\perp) r_\perp^{(2)}(\xi,k_\perp)} - 1 \right]^{-1} \right\}. \tag{16}$$

For separations $z > \lambda_p$ the Casimir pressure can be computed using either set of reflection coefficients, Eq. (13) or Eq. (14), with $\varepsilon(i\xi)$ or $Z(i\xi)$ given by Eq. (15). At the shortest separations $z < \lambda_p$ the impedance at characteristic frequencies is not small, and Eq. (13) should be used to calculate both the Casimir pressure and force. The most accurate results at these separations are obtained by using tabulated data for the imaginary part of the dielectric permittivity [58]. These data are substituted into the dispersion relation

$$\varepsilon(i\xi) = 1 + \frac{2}{\pi}\int_0^\infty \frac{\omega \mathrm{Im}\varepsilon(\omega)}{\omega^2 + \xi^2} d\omega \tag{17}$$

to obtain the dielectric permittivity along the imaginary frequency axis. The Casimir force, Eq. (12), and pressure, Eq. (16), can then be calculated as in Refs. [29,30]. This procedure was used here to calculate $F_C(z)$ and $P_C(z)$. The available tabulated data [58] were extended using the Drude model with the following plasma frequencies and relaxation parameters [29]: $\omega_p^{(1)} = 9.05$ eV, $\omega_p^{(2)} = 9.0$ eV, $\gamma^{(1)} = 30$ meV, $\gamma^{(2)} = 35$ meV, for Cu and Au, respectively. At large separations $z > \lambda_p$ our results almost coincide with those obtained in the framework of the plasma model given by Eq. (15). Note that at smaller separations $z < \lambda_p$ our results are practically independent of the chosen extrapolation and are completely determined by the available tabulated data.

It is useful to compare the calculated results for the real metals used with the ideal case when both sphere and plate were composed of a perfect metal with infinite conductivity. For example, the ratios of the calculated Casimir force to the force between an ideal sphere and plate are 0.467, 0.544, and 0.842 at separations $z = 70$ nm, 100 nm, and 500 nm, respectively. Similarly, the ratios of the calculated Casimir pressure between real plates to the pressure between ideal plates are 0.393, 0.468, and 0.799 for the same separations. These results are very close to those computed for Au-Au and Cu-Cu [29,30], which can be explained by the similarities of the optical data for Cu and Au.

B. Casimir pressure and force including surface roughness

As mentioned previously, the theoretical results obtained from Eqs. (12) and (16) take into account the finite conductivity of the boundary metals but neglect the effect of surface roughness. This effect, however, may constitute a correction of several tens of percent at the shortest separations depending on the character of the roughness. Hence, a precise computation of the Casimir force requires a careful characterization of the roughness as was performed in Sec. III A.

The roughness correction to the Casimir interaction is computed using the AFM images of the surfaces, such as the one shown in Fig. 6. As seen from Fig. 6, the characteristic longitudinal scale of the surface roughness is larger than the surface separation (especially in the region of the shortest separations where the effect of roughness is most significant). In this case the additive method [35,59] can be used to calculate the Casimir force taking account of roughness. As a result, the Casimir pressure between two plates with roughness corrections taken into account is given by

$$P_C(z) = \sum_{i,j=1}^{n} v_i v_j P_C(z + 2H_0 - h_i - h_j), \tag{18}$$

where v_i is defined in Sec. III A, $P_C(z)$ is given by Eq. (16), and the index i relates to one plate and j to the other. A plot of the relief heights h_i ($i = 1,2,\ldots,n = 59$) on the plate versus the fraction of the plate area w_i with height $h < h_{i+1}$ is shown in Fig. 7. It should be remembered that $H_0 = 35.46$ nm is the zero roughness level from which all separations z are measured (see Sec. III A). Note also that the separation distances $z + 2H_0 - h_i - h_j$ in Eq. (18) may be much smaller than λ_p for large relief heights h_i, h_j. Hence, one should use the optical tabulated data when calculating the finite conductivity corrections.

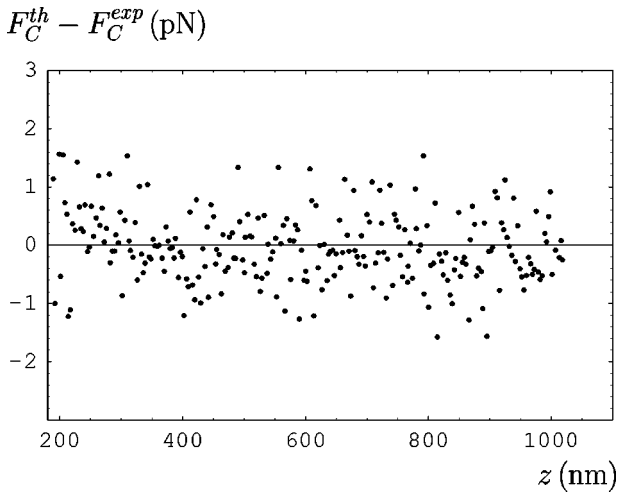

FIG. 10. Difference of the theoretical and experimental Casimir forces between the sphere and plate versus separation obtained from the static measurement.

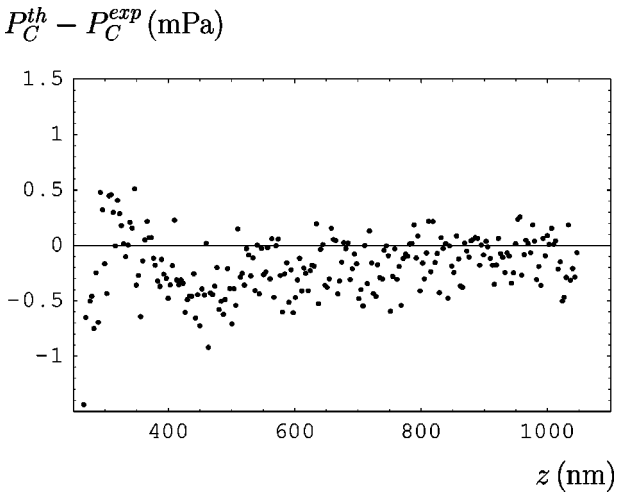

FIG. 11. Difference of the theoretical and experimental parallel plate Casimir pressures versus separation obtained from the dynamic measurement.

In a similar manner, the Casimir energy for two parallel plates with roughness is given by Eq. (18) after substituting E_C for P_C. It then follows that by the use of the proximity force theorem, the Casimir force for a sphere above a plate, accounting for both roughness and finite conductivity corrections, is given by

$$F_C(z)=\sum_{i,j=1}^{n} v_i v_j F_C(z+2H_0-h_i-h_j), \tag{19}$$

where $F_C(z)$ is given by Eq. (12).

We note that Eqs. (18) and (19) describe not only the separate effects of finite conductivity and surface roughness on the Casimir pressure and force, but also their combined effect. This is especially important at the shortest separations where the corrections are not small and cannot be represented as a product of two separate factors, one each for roughness and finite conductivity.

V. COMPARISON OF THEORY WITH EXPERIMENT AND TESTS OF ALTERNATIVE THERMAL CORRECTIONS

The theoretical Casimir force $F_C(z)$ acting between a sphere and a plate was computed using Eq. (19) for all separations where it was measured (19 sets of measurements containing $\approx$300 experimental points each). In Fig. 10 the difference between the theoretical and experimental force values

$$\Delta F_C(z_i)=F_C^{th}(z_i)-F_C^{exp}(z_i) \tag{20}$$

as a function of surface separation z_i is presented for one set of measurements. As can be seen from the figure, the values of $\Delta F_C(z_i)$ are clustered around $\Delta F_C(z_i)=0$, demonstrating good agreement between theory and experiment.

To quantify the level of agreement between theory and experiment we consider the root mean square deviation σ_N^F defined as

$$\sigma_N^F=\left\{\frac{1}{N}\sum_{i=1}^{N}\left[F_C^{th}(z_i)-F_C^{exp}(z_i)\right]^2\right\}^{1/2}, \tag{21}$$

where N is the number of points under consideration.

For example, if the first 250 points from all 19 sets of static measurements are considered (separations larger than 1 μm are not considered due to the large experimental relative error), one obtains $N=4750$, and $\sigma_{4750}^F\approx 0.6$ pN, which is less than the theoretical error (see below) but two times larger than the absolute error of the force measurements given by Eq. (10). The rms deviation depends slightly on the separation region under consideration. Thus, if separations $z\geqslant 400$ nm are considered, the first 185 points of all sets of measurements lead to $N=3515$, $\sigma_{3515}^F\approx 0.45$ pN. For one set of measurements shown in Fig. 10, $N=250$ and $\sigma_{250}^F \approx 0.66$ pN (close to the above value when all sets of measurements are considered). It can also be seen from Fig. 10 that there is a slight shift of the mean difference force value below the zero level equal to -0.045 pN, whose magnitude is much smaller than the absolute error of the force measurement.

A similar analysis was performed for the parallel plate Casimir pressure obtained from the dynamic measurement. The difference between the theoretical and experimental pressures $\Delta P_C(z_i)$ is defined as in Eq. (20), and the rms deviation σ_N^P is defined as in Eq. (21) with the substitution of F_C for P_C. Considering the first 235 points of all 5 sets of dynamic measurements one obtains $N=1175$, and $\sigma_{1175}^P \approx 0.5$ mPa. Once again, the rms deviation depends slightly on the separation interval. Thus, for 310 nm$\leqslant z\leqslant$420 nm (35 points), $N=175$ and $\sigma_{175}^P\approx 0.44$ mPa if all five sets of measurements are considered. For $z>310$ nm ($220\times 5 = 1100$ points), $\sigma_{1100}^P\approx 0.34$ mPa.

In Fig. 11, the quantity $\Delta P_C(z_i)$ is presented for one set of measurements ($N=235$). Here the shift of the mean difference pressure value below zero is equal to -0.26 mPa (whose magnitude is less than the absolute error of pressure

measurements). The rms deviation between theory and experiment in Fig. 11 is $\sigma_{235}^{P}\approx 0.43$ mPa, i.e., even less than for all five sets of dynamic measurements. Both Figs. 10 and 11 demonstrate good agreement between theory and experiment.

To estimate the theoretical precision, we consider other effects, in addition to finite conductivity and surface roughness, which were not taken into account in Eqs. (18), (19) for the Casimir pressure and force. Most prominent among these are finite-temperature corrections, which will be dealt with in detail later in this section. Another correction which should be considered arises from the fact that the plate used in the experiment is not infinite in extent. For the plate used, whose dimensions are 500×500 μm^2, this correction is evidently negligible if the sphere's center is located above the midpoint of the plate. However, in the configuration shown in Fig. 1, the sphere's center is above a point displaced from the right plate boundary by a distance $L=50$ μm. In this case, the Casimir force should be multiplied by a correction factor β that was found in Ref. [60],

$$\beta(z)=1-\frac{z^3}{R^3}\left(1-\frac{1}{\sqrt{1+L^2/R^2}}\right)^{-3}, \tag{22}$$

where R is the radius of the sphere. In our case, at the largest separation $z=1$ μm, this leads to $\beta=0.9865$. However, taking into account the fact that only one of the four sides of the plate is close to the sphere center projection reduces the correction factor to $\beta=0.997$. Thus, the correction is in fact less than 0.3%, and at a separation $z=500$ nm it is less than 0.04%. The same considerations apply to the pressure between two parallel plates. Consequently, the correction to the theoretical force and pressure due to the finiteness of the plate is much smaller than the uncertainty introduced by the sample-to-sample variation of the optical data. These sample-dependent variations in the index of refraction may lead to an error of $\approx 1\%$ [29,30]. An even smaller uncertainty is introduced into the computation by the effect of roughness when the topography of the surface is carefully characterized. A recently discussed correction due to the surface plasmon [61] is also not significant. The surface plasmon propagates when the frequency of the electromagnetic wave is greater than ω_p. Recall that in our case the shortest separations are 190 nm and 260 nm in the static and dynamic regimes, respectively. This leads to the highest characteristic frequencies $\omega_c=0.8\times 10^{15}$ rad/s and 0.6×10^{15} rad/s, respectively, which are 17 and 23 times, respectively, less than the plasma frequency for Au and Cu. As a result, the correction due to the surface plasmon in our case is much less than 1% even at shortest separations used.

As mentioned earlier, an important correction which may influence the magnitude of the Casimir interaction is due to the effect of nonzero temperature. This has been the subject of considerable controversy during the past few years (see, e.g., [32–35,42–44,56,62]). For an ideal metal the thermal correction can be determined using the Matsubara formulation of thermal quantum field theory (TQFT) [35,63–67]. The question is whether the thermal correction for good (but real) conductors is small at small separations, as is the case for ideal metals, or does it differ qualitatively from that for ideal metals. The approach of Refs. [32,33], which we call ''traditional'' since it yields results consistent with earlier studies of thermal effects, leads to a qualitatively identical thermal correction for real and ideal metals, as given by TQFT. For example, in the configuration of two parallel plates made of Cu and Au, the Casimir pressures at $z=300$ nm and $z=500$ nm at zero temperature are equal to -136 mPa and -17.0 mPa, respectively. The traditional thermal corrections [32,33] at room temperature $T=300$ K for these cases are equal to -0.00863 mPa and -0.00441 mPa, respectively. (For comparison, in the case of ideal metals, the corresponding Casimir pressures at $T=0$ K are equal to -160.43 mPa and -20.79 mPa, respectively, and the thermal correction at $T=300$ K is -0.00204 mPa and is independent of separation.) It is clearly seen that the traditional thermal corrections at room temperature are very small, and even the improved sensitivity of our experiment is not sufficient to measure them. Their contribution to the Casimir pressure is $\sim 0.006\%$ at $z=300$ nm and $\sim 0.03\%$ at $z=500$ nm, and can therefore be neglected.

The situation with the alternative thermal corrections, proposed in Refs. [42–44], is quite different. These corrections at separations $z>\lambda_p$ are much greater than those predicted by the traditional approach. According to Refs. [42,43], in the case of two parallel plates made of real metals there is an additional thermal correction linear in temperature given by

$$\Delta_T P_C^{(1)}(z)=\frac{k_B T}{16\pi z^3}\int_0^\infty y^2 dy\left[\frac{e^y}{r_\perp^{(1)}(0,y)r_\perp^{(2)}(0,y)}-1\right]^{-1}, \tag{23}$$

where

$$r_\perp^{(l)}(0,y)=\frac{y-\sqrt{y^2+4z^2\omega_p^{(l)2}}}{y+\sqrt{y^2+4z^2\omega_p^{(l)2}}}. \tag{24}$$

The effect of this correction is not as small as for the traditional approach. For example, at separations $z=300$ nm and 500 nm Eq. (23) leads to $\Delta_T P_C^{(1)}=4.89$ mPa and $\Delta_T P_C^{(1)}=1.23$ mPa, respectively, at $T=300$ K, i.e., to 3.6% and 7.24%, respectively, of the total Casimir pressure. Since these values far exceed the errors of the present experiment, the new results can be used as a decisive experimental test for the theoretical predictions made in Refs. [42,43].

In Fig. 12 the difference between the theoretical and experimental Casimir pressures $P_C^{th,1}-P_C^{exp}$ is presented as a function of separation for the same set of measurements as used in Fig. 11. Here, however, the theoretical pressure $P_C^{th,1}$ is computed using the alternative thermal correction given by Eq. (23). It is obvious that at separations $\lesssim 700$ nm the quantity $P_C^{th,1}-P_C^{exp}$ deviates significantly from zero. At the shortest separation $z=260$ nm this deviation reaches 5.5 mPa. Thus, the linear thermal correction to the Casimir pressure proposed in Refs. [42,43] is ruled out by the present experimental results. (Note that in a recent preprint [68]

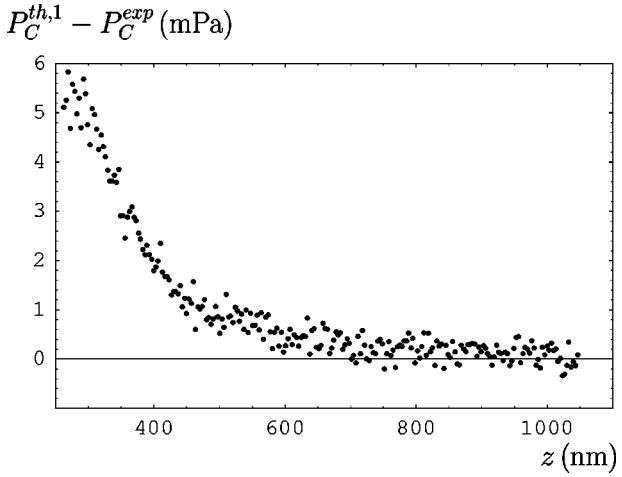

FIG. 12. Difference of the theoretical parallel plate Casimir pressure as predicted by Refs. [42,43] (which incorporates an alternative thermal correction) and experiment vs separation.

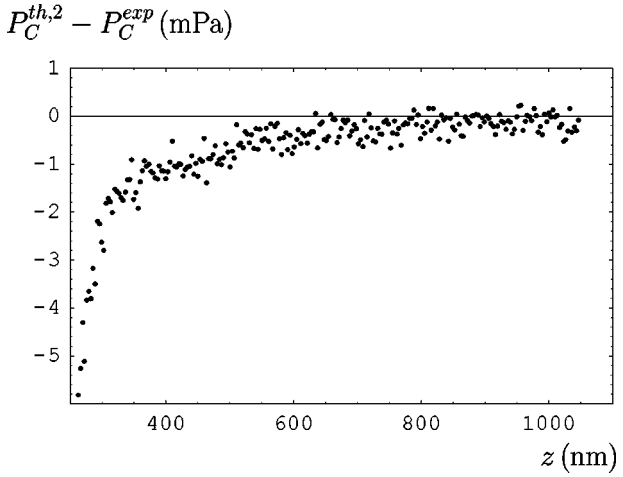

FIG. 13. Difference of the theoretical parallel plate Casimir pressures, as predicted by Ref. [44] (which incorporates another alternative thermal correction) and experiment vs separation.

qualitative arguments are presented on the role of the finite size of the plate and finite thickness of the gold layer. According to [68] these effects could lead to a 25% discrepancy between the experiment of Ref. [19], and the proposed alternative thermal correction [42,43] at a separation 1 μm.)

A second alternative thermal correction to the Casimir pressure between real metals was proposed in Ref. [44]. For our case of two metal plates it is expressed as

$$\Delta_T P_C^{(2)}(z) = -\frac{k_B T}{8\pi z^3}\zeta(3) + \Delta_T P_C^{(1)}(z), \tag{25}$$

where $\zeta(x)$ is the Riemann zeta-function, and $\Delta_T P_C^{(1)}(z)$ is defined in Eq. (23). This correction at $T=300$ K is also much larger than the traditional one for the separations used in our experiment. At the separation $z=300$ nm Eq. (25) leads to $\Delta_T P_C^{(2)} = -2.44$ mPa, i.e., to a 1.8% correction to the total Casimir pressure (the experimental precision at this separation is 0.43%). Thus, the present experiment also provides a test for the theoretical predictions of Ref. [44].

In Fig. 13 the difference between the theoretical and experimental Casimir pressures $P_C^{th,2} - P_C^{exp}$ is presented as a function of separation for the same set of measurements as in Fig. 11. Unlike Fig. 11, the theoretical pressure $P_C^{th,2}$ is computed using the second alternative thermal correction given by Eq. (25). As seen from Fig. 13, at separations less than 600 nm the quantity $P_C^{th,2} - P_C^{exp}$ deviates significantly from zero, and reaches 5 mPa at a separation $z=260$ nm. It follows that the thermal correction of Ref. [44] is also in contradiction with the results of the present experiment.

The conclusion that the alternative approaches to thermal corrections to the Casimir force do not agree with our experimental results is not surprising upon recognizing that the approaches of Refs. [42–44] violate the Nernst heat theorem [56]. To correctly describe the influence of thermal effects on the Casimir force between real (i.e., non-ideal) metals requires a proper understanding of the zero-frequency contribution in the Lifshitz formulas given by Eqs. (12) and (16). When the Drude dielectric function with a nonzero relaxation parameter is substituted into Eq. (13), the approach of Refs. [42,43] follows and the thermal correction given by Eq. (23) is found. If one then modifies the reflection coefficient $r_\perp(0,k_\perp)$ by setting it equal to unity (as for real photons), the thermal correction (25) is obtained [44]. However, to avoid contradictions with fundamental physical principles and experiment, it is necessary to start from the physical behavior of the surface impedance in the appropriate range of characteristic frequencies (i.e., infrared optics in our case), and to extrapolate to zero frequency [34]. Under these conditions, the traditional thermal correction between real metals is recovered, and this thermal correction is in agreement with both thermodynamics and the present experiments. Furthermore, it transforms smoothly into the limiting case of ideal metals as described by the Matsubara formulation of TQFT.

To conclude this section, the theoretical uncertainty, which is $\approx 1\%$ of the Casimir force or pressure, exceeds the experimental uncertainty at the shortest separations used in this experiment (0.27% for the force at 188 nm and 0.26% for the pressure at 260 nm). However, at separations $z > 370$ nm the experimental uncertainties exceed the theoretical uncertainties. Within the achieved levels of precision there is good agreement between theory and experiment over the entire measurement range.

VI. CONSTRAINTS ON NEW YUKAWA FORCES AND EXTRA-DIMENSIONAL PHYSICS

As mentioned in the Introduction, in many extensions to the standard model, including theories with large compact extra dimensions [1], the potential energy between two point masses m_1 and m_2 separated by a distance r is given by the usual Newtonian potential with a Yukawa correction [1,12,13],

$$V(r) = -\frac{G m_1 m_2}{r}(1 + \alpha e^{-r/\lambda}), \tag{26}$$

where α is a dimensionless constant characterizing the strength of the Yukawa force, and λ is its range. For theories with $n \gg 1$ extra dimensions $\alpha \sim 1$ and $\lambda \sim R_n$, where R_n is the size of the compact dimensions, Eq. (26) holds under the condition [1]

$$r \gg R_n \sim \frac{1}{M_{Pl}^{(N)}} \left(\frac{M_{Pl}}{M_{Pl}^{(N)}} \right)^{2/n} \sim 10^{32/n-17} \text{ cm}. \quad (27)$$

For $n=1$ it follows from Eq. (27) that $R_1 \sim 10^{15}$ cm which is excluded by solar system tests of Newtonian gravity [69]. If, however, $n=2$ or $n=3$, the sizes of extra dimensions are $R_2 \sim 1$ mm or $R_3 \sim 5$ nm, respectively. While recent gravity experiments have investigated millimeter distance scales without finding evidence of new physics, gravity remains poorly tested at scales $\lesssim 10^{-4}$ m (see Ref. [70] for a review).

For models of non-compact (but warped) extra dimensions [2] the potential energy takes the form of the Newtonian potential with a power-law correction

$$V(r) = -\frac{Gm_1m_2}{r} \left(1 + \frac{2}{3k^2r^2} \right), \quad (28)$$

where $r \gg 1/k$ and $1/k$ is the warping scale. The correction in Eq. (28) can be generalized to arbitrary inverse powers,

$$V_l(r) = -\frac{Gm_1m_2}{r} \left[1 + \alpha_l \left(\frac{r_0}{r} \right)^{l-1} \right], \quad (29)$$

where α_l is a dimensionless constant, l is a positive integer, and $r_0 = 10^{-15}$ m.

We note that Yukawa and power-law corrections given in Eqs. (26) and (29) also arise in ways unrelated to extra-dimensional physics. For example, the Yukawa potential describes new forces generated by the exchange of light bosons of mass $\mu = 1/\lambda$, such as scalar axions, graviphotons, hyperphotons, dilatons, and moduli among others (see, e.g., [69–73]). For such forces the interaction constant α could be much larger than unity. Power-law corrections, as in Eq. (29), arise from the simultaneous exchange of two photons or two massless scalars ($l=2$ [74]), two massless pseudoscalars ($l=3$ [75,76]), and from the exchange of a massless axion or a massless neutrino-antineutrino pair ($l=5$ [76,77]).

The agreement between theory and experiment for our Casimir force measurements can be used to set new constraints on the Yukawa strength α as a function of λ from Eq. (26). The total force acting between a sphere and a plate due to the potential described by Eq. (26) is obtained by integration over the volumes of the sphere and the plate, and subsequent differentiation with respect to z. In fact, the contribution of the Newtonian gravitational force is very small and can be neglected. To prove this, let us consider a sphere above the center of an enlarged plate modelled by a disk with a radius $L_0 \gg R = 294.3$ μm. (In the present experiment the projection of the sphere center is displaced by 450 μm from one edge of the plate, and by 50 μm from the other.) In this case the Newtonian gravitational force is given by [39]

$$F_N \approx -\frac{8}{3}\pi^2 G \rho_{disk} \rho_{sphere} D R^3 \left(1 - \frac{D}{2L_0} - \frac{R}{L_0} \right), \quad (30)$$

where $D = 3.5$ μm is the thickness of the plate. To obtain an upper limit, let us neglect the layered structure of both test bodies and set $L_0 \to \infty$, $\rho_{disk} = \rho_{\text{Cu}} = 8.93 \times 10^3$ kg/m^3, and $\rho_{sphere} = \rho_{\text{Au}} = 19.28 \times 10^3$ kg/m^3. It then follows from Eq. (30) that $F_N \approx -3.2 \times 10^{-17}$ N. This value is four orders of magnitude smaller than the absolute error of the force measurement in the static regime. Hence, the contribution of the Newtonian gravitational force can be neglected at this stage.

For a Yukawa force between a sphere and a plate, the constraints should be calculated considering the detailed structure of the sphere and plate. The sphere of density $\rho_s = 4.1 \times 10^3$ kg/m^3 was coated with a layer of Cr of thickness $\Delta_{\text{Cr}} = 1$ nm with $\rho_{\text{Cr}} = 7.19 \times 10^3$ kg/m^3, and a layer of Au of thickness $\Delta_{\text{Au}} = 203$ nm. The plate of density $\rho_{\text{Si}} = 2.33 \times 10^3$ kg/m^3 was coated first with the same thickness of Cr and then with a layer of Cu of thickness $\Delta_{\text{Cu}} = 200$ nm. Considering that the conditions $z, \lambda \ll R, D$ are satisfied, the hypothetical force is given by [35,36]

$$\begin{aligned} F^{hyp}(z) = &-4\pi^2 G \alpha \lambda^3 e^{-z/\lambda} R [\rho_{\text{Au}} - (\rho_{\text{Au}} - \rho_{\text{Cr}}) e^{-\Delta_{\text{Au}}/\lambda} \\ &- (\rho_{\text{Cr}} - \rho_s) e^{-(\Delta_{\text{Au}} + \Delta_{\text{Cr}})/\lambda}] [\rho_{Cu} - (\rho_{Cu} - \rho_{\text{Cr}}) \\ &\times e^{-\Delta_{Cu}/\lambda} - (\rho_{\text{Cr}} - \rho_{Si}) e^{-(\Delta_{Cu} + \Delta_{\text{Cr}})/\lambda}]. \end{aligned} \quad (31)$$

In our experiment, the strongest constraints on the Yukawa hypothetical interactions are obtained from the dynamic measurement of the parallel plate pressure (i.e., Casimir force gradient) rather than the static measurement of the Casimir force. For this case, the Yukawa pressure can be found from Eq. (31) by using Eq. (6), which follows from the proximity force theorem, Eq. (5),

$$\begin{aligned} P^{hyp}(z) = &-2\pi G \alpha \lambda^2 e^{-z/\lambda} [\rho_{\text{Au}} - (\rho_{\text{Au}} - \rho_{\text{Cr}}) e^{-\Delta_{\text{Au}}/\lambda} \\ &- (\rho_{\text{Cr}} - \rho_s) e^{-(\Delta_{\text{Au}} + \Delta_{\text{Cr}})/\lambda}] [\rho_{Cu} - (\rho_{Cu} - \rho_{\text{Cr}}) \\ &\times e^{-\Delta_{Cu}/\lambda} - (\rho_{\text{Cr}} - \rho_{Si}) e^{-(\Delta_{Cu} + \Delta_{\text{Cr}})/\lambda}]. \end{aligned} \quad (32)$$

Note that the Newtonian gravitational pressure is also below the sensitivity of the present experiment and can be neglected.

As shown in Ref. [36], surface roughness can significantly influence the magnitude of a hypothetical force in the nanometer range. To compute the hypothetical pressure taking account of roughness, one can use exactly the same method that was applied in Sec. IV in the case of the Casimir pressure. The result is

$$P_R^{hyp}(z) = \sum_{i,j=1}^{n} v_i v_j P^{hyp}(z + 2H_0 - h_i - h_j), \quad (33)$$

where our notation is that of Sec. IV, and P^{hyp} is given by Eq. (32).

With these results, we can now obtain constraints on the hypothetical Yukawa pressure from the agreement of our measurements of the Casimir pressure with theory. According to the results of Sec. V, the optimal separation region for

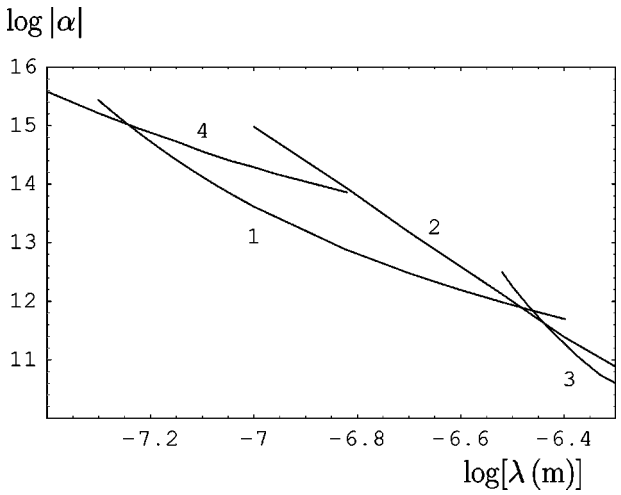

FIG. 14. Constraints on the Yukawa interaction constant α vs interaction range λ. Curve 1 is obtained in this paper, curve 2 follows from old measurements of the Casimir force between dielectrics [35]. Curves 3 and 4 are obtained from the Casimir force measurements between metals by use of the torsion pendulum [19,36] and by means of an atomic force microscope, [23,39] respectively. The region in the (α,λ) plane above each curve is excluded, and below each curve is allowed.

obtaining constraints is $z>310$ nm. Here the rms deviation between theory and experiment, $\sigma^P_{1100}=0.34$ mPa, is somewhat smaller than would be the case if the complete measurement range were used, which includes the shortest separations 260 nm$\leqslant z\leqslant$310 nm. (At the shortest separations the experimental relative error is less than the theoretical error, but it increases with separation so it eventually exceeds the theoretical relative error.) Within the interval $z>310$ nm the strongest constraints are obtained from the shortest separations. We choose $z_0=320$ nm and obtain constraints from the inequality

$$|P^{hyp}_R(z_0)|\leqslant\sigma^P_{1100}=0.34\ \ \text{mPa}. \tag{34}$$

In Fig. 14 constraints on α following from Eq. (34) are plotted for different values of the interaction range λ (curve 1). In the same figure constraints from previous experiments are also shown. They were obtained from old measurements of the Casimir force between dielectrics [35] (curve 2), from Casimir force measurements by means of a torsion pendulum [19,36] (curve 3), and by the use of an AFM [23,36,39] (curve 4). In all cases the region in the (α,λ) plane above the curve is excluded, and below the curve is allowed by the experimental results. As can be seen from Fig. 14, the present experiment leads to the strongest constraints in a wide interaction range, 56 nm$\leqslant\lambda\leqslant$330 nm. The largest improvement, by a factor of 11, is achieved at $\lambda\approx150$ nm. We note that the constraints obtained here almost completely fill in the gap between the modern constraints obtained by AFM measurements, and those obtained using a torsion pendulum. Within this gap the best previous constraints were obtained from old measurements of the Casimir force between dielectrics which are not as precise or reliable as those obtained here from the Casimir pressure measurements between metals using a MTO.

Turning to the power-law-type hypothetical interactions given by Eq. (29), the present experiment does not lead to improved constraints. This is explained by the fact that the metallic coatings used were too thin (and hence, too light) to give a significant contribution to hypothetical interactions with a longer interaction range. In fact, the thicker (bulk) matter contributes more significantly in this case, even though its density is much lower than for the metal coatings. To obtain stronger constraints on the constants characterizing new power-law interactions, thicker metal coatings and larger interacting bodies are preferable. We anticipate that future measurements of the Casimir force will employ such samples.

VII. CONCLUSIONS AND DISCUSSION

Our primary objective in the present paper has been to set new limits on extra-dimensional models and other physics beyond the standard model using Casimir force measurements between a sphere and a plate separated by $\sim$0.2–1.2 μm. These experimental results along with a detailed theoretical analysis lead to new constraints on Yukawa modifications of Newtonian gravity at short distances, and these are presented in Fig. 14.

Although the constraints on the Yukawa parameter α we obtain are $\sim10^{13}$, this does not imply that our experiment has to be improved by 13 orders of magnitude to detect Newtonian gravity. Rather, the exponential factor $e^{-r/\lambda}$ in Eq. (26) strongly suppresses contributions from those parts of the sphere and plate separated by $\gtrsim\lambda$. This ''finite size effect'' [69], which is not relevant for gravity, has a consequence that a Yukawa force between the sphere and plate with $\alpha=1$ is much weaker than gravity. The actual gravitational force in our experiment is only ~5 orders of magnitude from being detected (using the actual materials employed), a gap that may be closed within the forseeable future based on the rapid progress various groups have made in the past few years.

To carry out our objective, a MTO was used to obtain the first precise measurements of the Casimir force between dissimilar metals Cu and Au. In the static regime, the Casimir force between a sphere and a plate was measured with an absolute error 0.3 pN at a 95% confidence level. This translates into an experimental relative error of the Casimir force measurements at the separation 188 nm of $\approx$0.27%, i.e., several times smaller than the most precise previous experiments carried out by means of an AFM [20–23]. To take advantage of the high quality factor of the MTO, the Casimir force derivative between the sphere and plate was then measured dynamically. This derivative was shown to be effectively equivalent to the pressure between two parallel plates composed of the same materials. This pressure was determined with a mean absolute error of 0.6 mPa at the same confidence level, which leads to an experimental relative error of $\approx$0.26% at the separation 260 nm. (This compares with a relative error of 15% quoted by the authors of Ref.

[26] who directly measured the Casimir pressure between parallel plates.)

As noted above, the precise calculation of the Casimir force and pressure between real metals that is needed to extract the effects of new physics calls for the careful accounting of different corrections (e.g., due to surface roughness, finite conductivity of the boundary metals, nonzero temperature, and finite extent of the plate). The corrections due to roughness were computed on the basis of the AFM images of the surfaces of the test bodies. Finite conductivity corrections were calculated using tabulated data for the complex index of refraction. Other corrections were also estimated (including traditional thermal corrections) and found to be negligible. The estimated theoretical uncertainty is at the level of 1% of the calculated force, i.e., greater than the experimental uncertainty at the shortest separations used. Within the limits of all errors, theory is in good agreement with experiment.

The level of agreement between theory and experiment was used to draw important conclusions concerning the influence of thermal effects on the Casimir force predicted by quantum field theory at nonzero temperature. Our experimental results lead to a resolution of the controversy over whether the thermal effects on the Casimir force between real metals are close to those predicted by the Matsubara formulation of quantum field theory for ideal metals, or are significantly different as claimed in Refs. [42–44]. We have shown that the experimental results contradict the large, linear in temperature, thermal corrections predicted in Refs. [42–44]. Although the sensitivity of the current experiment is not yet sufficient to detect the small thermal corrections to the Casimir force and pressure predicted for real metals in Refs. [32,33], these corrections are compatible with our experiment.

The good agreement between theory and experiment was then used to set stronger constraints on hypothetical Yukawa interactions predicted by extra-dimensional physics and extensions to the standard model. Existing limits were strengthened by a factor of up to 11 within a wide interaction range, from 56 nm to 330 nm. This interaction range covers the gap between the modern results obtained from Casimir force measurements using a torsion pendulum and an AFM. The previously known constraints within this gap were based on old, and less reliable, Casimir force measurements between dielectrics.

Our experimental arrangement suggests the need for additional work to further improve the agreement between theory and experiment. We plan to use smoother and thicker metal coatings on the surfaces of the test bodies, yielding a better characterization of the roughness. This will permit us to carry out measurements at shorter separations, and to significantly strengthen the constraints on the predictions of extra-dimensional physics in a wider interaction range. The ultimate goal of this program is to use the iso-electronic effect [18,39,78–80] to suppress the Casimir force so as to improve our sensitivity to new forces beyond the standard model.

ACKNOWLEDGMENTS

R.S.D. acknowledges financial support from the Petroleum Research Foundation through ACS-PRF Grant No. 37542-G. The work of E.F. is supported in part by the U.S. Department of Energy under Contract No. DE-AC02-76ER071428. G.L.K. and V.M.M. are grateful to the Department of Physics, Purdue University for kind hospitality. They were partially supported by CNPq and Finep (Brazil).

[1] N. Arkani-Hamed, S. Dimopoulos, and G. Dvali, Phys. Lett. B **429**, 263 (1998); Phys. Rev. D **59**, 086004 (1999); I. Antoniadis, N. Arkani-Hamed, S. Dimopoulos, and G. Dvali, Phys. Lett. B **436**, 257 (1998).

[2] L. Randall and R. Sundrum, Phys. Rev. Lett. **83**, 3370 (1999); **83**, 4690 (1999).

[3] B. Abbott *et al.*, Phys. Rev. Lett. **86**, 1156 (2001).

[4] P. Abreu *et al.*, Phys. Lett. B **485**, 45 (2000).

[5] C. Adloff *et al.*, Phys. Lett. B **479**, 358 (2000).

[6] C. Hanhart, D.R. Phillips, S. Reddy, and M.J. Savage, Nucl. Phys. **B595**, 335 (2001).

[7] S. Hannestad and G.G. Raffelt, Phys. Rev. Lett. **87**, 051301 (2001).

[8] S. Cassisi, V. Castellani, S. Degl'Innocenti, G. Fiorentini, and R. Ricci, Phys. Lett. B **481**, 323 (2000).

[9] L.J. Hall and D. Smith, Phys. Rev. D **60**, 085008 (1999).

[10] M. Fairbairn, Phys. Lett. B **508**, 335 (2001).

[11] S. Hannestad, Phys. Rev. D **64**, 023515 (2001).

[12] A. Kehagias and K. Sfetsos, Phys. Lett. B **472**, 39 (2000).

[13] E.G. Floratos and G.K. Leontaris, Phys. Lett. B **465**, 95 (1999).

[14] G.L. Smith, C.D. Hoyle, J.H. Gundlach, E.G. Adelberger, B.R. Heckel, and H.E. Swanson, Phys. Rev. D **61**, 022001 (2000).

[15] C.D. Hoyle, U. Schmidt, B.R. Heckel, E.G. Adelberger, J.H. Gundlach, D.J. Kapner, and H.E. Swanson, Phys. Rev. Lett. **86**, 1418 (2001).

[16] J.C. Long, H.W. Chan, A.B. Churnside, E.A. Gulbis, M.C.M. Varney, and J.C. Price, Nature (London) **421**, 922 (2003).

[17] J. Chiaverini, S.J. Smullin, A.A. Geraci, D.M. Weld, and A. Kapitulnik, Phys. Rev. Lett. **90**, 151101 (2003).

[18] D. E. Krause and E. Fischbach, in *Gyroscopes, Clocks, and Interferometers: Testing General Relativity in Space*, edited by C. Lämmerzahl, C. W. F. Everitt, and F. W. Hehl (Springer-Verlag, Berlin, 2001).

[19] S.K. Lamoreaux, Phys. Rev. Lett. **78**, 5 (1997); **81**, 5475(E) (1998).

[20] U. Mohideen and A. Roy, Phys. Rev. Lett. **81**, 4549 (1998); G.L. Klimchitskaya, A. Roy, U. Mohideen, and V.M. Mostepanenko, Phys. Rev. A **60**, 3487 (1999).

[21] A. Roy, C.-Y. Lin, and U. Mohideen, Phys. Rev. D **60**, 111101 (1999).

[22] A. Roy and U. Mohideen, Phys. Rev. Lett. **82**, 4380 (1999).

[23] B.W. Harris, F. Chen, and U. Mohideen, Phys. Rev. A **62**, 052109 (2000).

[24] T. Ederth, Phys. Rev. A **62**, 062104 (2000).
[25] H.B. Chan, V.A. Aksyuk, R.N. Kleiman, D.J. Bishop, and F. Capasso, Science **291**, 1941 (2001); Phys. Rev. Lett. **87**, 211801 (2001).
[26] G. Bressi, G. Carugno, R. Onofrio, and G. Ruoso, Phys. Rev. Lett. **88**, 041804 (2002).
[27] F. Chen, U. Mohideen, G.L. Klimchitskaya, and V.M. Mostepanenko, Phys. Rev. Lett. **88**, 101801 (2002); Phys. Rev. A **66**, 032113 (2002).
[28] F. Chen, G. L. Klimchitskaya, U. Mohideen, and V. M. Mostepanenko (unpublished).
[29] A. Lambrecht and S. Reynaud, Eur. Phys. J. D **8**, 309 (2000).
[30] G.L. Klimchitskaya, U. Mohideen, and V.M. Mostepanenko, Phys. Rev. A **61**, 062107 (2000).
[31] V.B. Bezerra, G.L. Klimchitskaya, and V.M. Mostepanenko, Phys. Rev. A **62**, 014102 (2000).
[32] C. Genet, A. Lambrecht, and S. Reynaud, Phys. Rev. A **62**, 012110 (2000).
[33] M. Bordag, B. Geyer, G.L. Klimchitskaya, and V.M. Mostepanenko, Phys. Rev. Lett. **85**, 503 (2000); **87**, 259102 (2001).
[34] B. Geyer, G.L. Klimchitskaya, and V.M. Mostepanenko, Phys. Rev. A **67**, 062102 (2003).
[35] M. Bordag, U. Mohideen, and V.M. Mostepanenko, Phys. Rep. **353**, 1 (2001).
[36] M. Bordag, B. Geyer, G.L. Klimchitskaya, and V.M. Mostepanenko, Phys. Rev. D **58**, 075003 (1998); **60**, 055004 (1999); **62**, 011701(R) (2000).
[37] J.C. Long, H.W. Chan, and J.C. Price, Nucl. Phys. **B539**, 23 (1999).
[38] V.M. Mostepanenko and M. Novello, Phys. Rev. D **63**, 115003 (2001).
[39] E. Fischbach, D.E. Krause, V.M. Mostepanenko, and M. Novello, Phys. Rev. D **64**, 075010 (2001).
[40] R.S. Decca, D. López, E. Fischbach, and D.E. Krause, Phys. Rev. Lett. **91**, 050402 (2003).
[41] E.M. Lifshitz, Zh. Éksp. Teor. Fiz. **29**, 94 (1956) [Sov. Phys. JETP **2**, 73 (1956)].
[42] M. Boström and B.E. Sernelius, Phys. Rev. Lett. **84**, 4757 (2000).
[43] J.S. Høye, I. Brevik, J.B. Aarseth, and K.A. Milton, Phys. Rev. E **67**, 056116 (2003).
[44] V.B. Svetovoy and M.V. Lokhanin, Phys. Lett. A **280**, 177 (2001).
[45] C.A. Bolle *et al.*, Nature (London) **399**, 43 (1999).
[46] S. D. Senturia, *Microsystem Design* (Kluwer, Boston, 2001).
[47] F. Ayela *et al.*, Rev. Sci. Instrum. **71**, 2211 (2000).
[48] M. L. Roukes, Solid-State Sensor and Actuator Workshop, Hilton Head Island, South Carolina, 2000.
[49] W. R. Smythe, *Static and Dynamic Electricity* (McGraw-Hill, New York, 1939).
[50] R.S. Decca, H.D. Drew, and K.L. Empson, Rev. Sci. Instrum. **68**, 1291 (1997).
[51] J. Blocki *et al.*, Ann. Phys. (N.Y.) **105**, 427 (1977).
[52] B.V. Derjaguin, I.I. Abrikosova, and E.M. Lifshitz, Q. Rev., Chem. Soc. **10**, 295 (1956).
[53] B. Geyer, G.L. Klimchitskaya, and V.M. Mostepanenko, Phys. Rev. A **65**, 062109 (2002).
[54] M. Schaden and L. Spruch, Phys. Rev. A **58**, 935 (1998).
[55] P. Johansson and P. Apell, Phys. Rev. B **56**, 4159 (1997).
[56] V.B. Bezerra, G.L. Klimchitskaya, and V.M. Mostepanenko, Phys. Rev. A **66**, 062109 (2002).
[57] V.B. Bezerra, G.L. Klimchitskaya, and C. Romero, Phys. Rev. A **65**, 012111 (2002).
[58] *Handbook of Optical Constants of Solids*, edited by E. D. Palik (Academic, New York, 1998).
[59] T. Emig, A. Hanke, R. Golestanian, and M. Kardar, Phys. Rev. Lett. **87**, 260402 (2001).
[60] V.B. Bezerra, G.L. Klimchitskaya, and C. Romero, Mod. Phys. Lett. A **12**, 2613 (1997).
[61] R. Esquivel, C. Villareal, and W. L. Mochán, Phys. Rev. A **68**, 052103 (2003).
[62] F. Chen, G.L. Klimchitskaya, U. Mohideen, and V.M. Mostepanenko, Phys. Rev. Lett. **90**, 160404 (2003).
[63] J. Mehra, Physica (Amsterdam) **37**, 145 (1967).
[64] L.S. Brown and G.J. Maclay, Phys. Rev. **184**, 127 (1969).
[65] P. W. Milonni, *The Quantum Vacuum* (Academic, San Diego, 1994).
[66] V. M. Mostepanenko and N. N. Trunov, *The Casimir Effect and its Applications* (Clarendon, Oxford, 1997).
[67] K. A. Milton, *The Casimir Effect* (World Scientific, Singapore, 2001).
[68] J.R. Torgerson and S.K. Lamoreaux, quant-ph/0309153.
[69] E. Fischbach and C. L. Talmadge, *The Search for Non-Newtonian Gravity* (Springer-Verlag, New York, 1999).
[70] E.G. Adelberger, B.R. Heckel, and A.E. Nelson, hep-ph/0307284.
[71] Y. Fujii, Int. J. Mod. Phys. A **6**, 3505 (1991).
[72] E.G. Adelberger, B.R. Heckel, C.W. Stubbs, and W.F. Rogers, Annu. Rev. Nucl. Part. Sci. **41**, 269 (1991).
[73] S. Dimopoulos and G.F. Giudice, Phys. Lett. B **379**, 105 (1996).
[74] J. Sucher and G. Feinberg, in *Long-Range Casimir Forces*, edited by F. S. Levin and D. A. Micha (Plenum, New York, 1993).
[75] S.D. Drell and K. Huang, Phys. Rev. **91**, 1527 (1953).
[76] F. Ferrer and J.A. Grifols, Phys. Rev. D **58**, 096006 (1998).
[77] G. Feinberg and J. Sucher, Phys. Rev. **166**, 1638 (1968); E. Fischbach, Ann. Phys. (N.Y.) **247**, 213 (1996); S.D.H. Hsu and P. Sikivie, Phys. Rev. D **49**, 4951 (1994).
[78] E. Fischbach, S.W. Howell, S. Karunatillake, D.E. Krause, R. Reifenberger, and M. West, Class. Quantum Grav. **18**, 2427 (2001).
[79] D.E. Krause and E. Fischbach, Phys. Rev. Lett. **89**, 190406 (2002).
[80] E. Fischbach, D. E. Krause, R. S. Decca, and D. López, Phys. Lett. A **318** 165 (2003).